HHS Public Access

Author manuscript

Dev Neurobiol. Author manuscript; available in PMC 2017 April 01.

Published in final edited form as:

Dev Neurobiol. 2016 April ; 76(4): 452–469. doi:10.1002/dneu.22326.

EphA7 Regulates Spiral Ganglion Innervation of Cochlear Hair Cells

Young J. Kim[1,4], **Leena A. Ibrahim**[1,4], **Sheng-zhi Wang**[1], **Wei Yuan**[6,*], **Oleg V. Evgrafov**[1,5], **James A. Knowles**[1,5], **Kai Wang**[1,5], **Huizhong W. Tao**[1,3], and **Li I. Zhang**[1,2,*]

[1]Zilkha Neurogenetic Institute, Keck School of Medicine, University of Southern California, Los Angeles, California 90033, USA

[2]Department of Physiology and Biophysics, University of Southern California, Keck School of Medicine, Los Angeles, California, USA

[3]Department of Cell and Neurobiology, Keck School of Medicine, University of Southern California, Los Angeles, California, USA

[4]Neuroscience Graduate Program, University of Southern California, Los Angeles, California, USA

[5]Department of Psychiatry, Keck School of Medicine, University of Southern California, Los Angeles, California, USA

[6]Department of Otolaryngology of Southwest Hospital, Third Military Medical University, Chongqing 400038, China

Abstract

During the development of periphery auditory circuitry, spiral ganglion neurons (SGNs) form a spatially precise pattern of innervation of cochlear hair cells (HCs), which is an essential structural foundation for central auditory processing. However, molecular mechanisms underlying the developmental formation of this precise innervation pattern remain not well understood. Here, we specifically examined the involvement of Eph family members in cochlear development. By performing RNA-sequencing for different types of cochlear cell, *in situ* hybridization and immunohistochemistry, we found that EphA7 was strongly expressed in a large subset of SGNs. In EphA7 deletion mice, there was a reduction in the number of inner radial bundles originating from SGNs and projecting to HCs as well as in the number of ribbon synapses on inner hair cells (IHCs), as compared with wild-type or heterozygous mutant mice, attributable to fewer type I afferent fibers. The overall activity of the auditory nerve in EphA7 deletion mice was also reduced, although there was no significant change in the hearing intensity threshold. *In vitro* analysis further suggested that the reduced innervation of HCs by SGNs could be attributed to a role of EphA7 in regulating outgrowth of SGN neurites, as knocking down EphA7 in SGNs resulted in diminished SGN fibers. In addition, suppressing the activity of ERK1/2, a potential downstream target of EphA7 signaling, either with specific inhibitors in cultured explants or by knocking out Prkg1, also resulted in reduced SGN fibers. Together, our results suggest that EphA7 plays an important role in the developmental formation of cochlear innervation pattern through controlling

*Correspondence should be addressed to: L.I. Zhang (liizhang@usc.edu).

SGN fiber ontogeny. Such regulation may contribute to the salience level of auditory signals presented to the central auditory system.

Keywords

Peripheral auditory system; cochlear development; hair cell; spiral ganglion; axon guidance molecule

INTRODUCTION

During cochlear development, spiral ganglion neurons (SGNs) form a precise, stereotypic pattern of innervation of hair cells (HCs). Molecular mechanisms underlying the formation of this innervation pattern remain unclear. Several studies have begun to examine the role of various axon guidance molecules in this process. It has been found that Slit/Robo family molecules (Wang et al., 2013), and ErbB2 (Mao et al., 2014) are involved in controlling the migration of SGNs during the formation of the HC innervation pattern. Recently, it was also reported that ephrins and Eph receptors are involved in the regulation of SGN axons projecting to HCs (Coate et al., 2012; Defourny et al., 2013).

Ephrins and Eph receptors play a variety of roles during the establishment of neural circuitry. Their varied expressions in a spatially organized manner during development provide specific Eph/ephrin interactions for regulating cell migration, neurite outgrowth, axon guidance, synaptogenesis, and many more (Pasquale, 2005). Various studies have shown that ephrins and Eph receptors are expressed in the developing mouse inner ear (Bianchi and Liu, 1999; Bianchi and Gale, 1998; Pickles et al., 2002; Pickles, 2003; Saeger et al., 2011; Zhou et al., 2011) and that they are involved in the proper assembly of auditory neural circuits at nearly every stage of the auditory pathway from peripheral projections to the auditory cortex (for review, see Cramer and Gabriele, 2014).

Recent studies have shed some light on ephrin signaling mechanisms for regulating peripherally projecting axons of SGNs that innervate HCs. Eph receptor A4 (EphA4) has been found to be important for the proper fasciculation of SGN axons, and for their proper pathfinding to innervate HCs (Coate et al., 2012; Defourny et al., 2013). EphB1–3 are shown to regulate the growth of SGN axons (Bianchi and Gray, 2002; Zhou et al., 2011). Interestingly, the defect caused by each specific Eph receptor mutation is relatively subtle. Given the fact that there are eight EphA and five EphB receptor variants, this raises a possibility that Eph receptors may act synergistically to control coordinated development of cochlear innervation pattern. Indeed, previous *in situ* hybridization studies have shown expression of several Eph members other than EphA4 and EphB1–3 in the developing mouse inner ear (Bianchi and Gale, 1998; Bianchi and Liu, 1999; Pickles, 2003).

To systematically examine the involvement of different Eph receptors in cochlear development, we generated gene expression profiles of Eph receptors in different cochlear cell populations and observed strong expression of EphA7 in the spiral ganglion (SG) and greater epithelial ridge (GER). In the EphA7 knockout mouse, the number of SGN fibers was affected, as evidenced by a reduced number of inner fiber bundles and diminished

synaptic contacts on inner hair cells. Our results revealed a previously unrecognized role of EphA7 in regulating the initial elaboration of SGN neurites, and suggested possible Eph/ephrin mediated processes in a specific subset of SGNs.

METHODS

Animals

Mice were handled according to the protocols approved by the Institutional Animal Care and Use Committees at the University of Southern California (USC). EphA7 and Prkg1 homozygous mutants were obtained by crossing heterozygous littermates with the plug day defined as E0.5. Genotyping was performed as previously described (Rashid et al., 2005). Genotyping of Ai6 (Rosa-CAG-LSL-ZsGreen1-WPRE), Parvalbumin (PV)-Cre, glutamate decarboxylase 1 (Gad1)-GFP mice (The Jackson Laboratory) was performed following previous studies (Hippenmeyer et al., 2005; Madisen et al., 2010; Tamamaki et al., 2003).

Tissue dissection, FACS, RNA amplification, and RNA sequencing

Mouse cochleae were dissected from P3 to P7 pups. Gad1-GFP cochleae were used for GER cells, and PV-Cre::Ai6 cochleae for HCs and SGNs. Tissues were further treated to achieve complete dissociation as described previously (Wang et al., 2013). Fluorescence-activated cell sorting (FACS) was performed at the Flow Cytometry Core Facility of USC. Cell suspensions were fed into a BDAriaII sorter and purified using 488 nm laser excitation and a 100-μm cytoNozzle. Distinct cell populations were collected into DMEM plus 10% FBS and pelleted down through centrifuge. RNA was extracted from the collected cells using PicoPure RNA isolation kit (Arcturus). Each RNA sample was then amplified using WT-Ovation Pico amplification kit (Nugen). The quantity and quality of isolated RNAs were determined with NanoDrop 2000 (NanoDrop Technologies) and confirmed by Bioanalyzer 2100 (Agilent Technologies). RNA-sequencing was conducted with Illumina HiSeq 2000 (Illumina) at the USC Genomics Center following the manufacturer's instructions.

Immunohistochemistry

Mouse cochleae were dissected at desired time points and fixed with 4% PFA for 2–24hours. Fixed samples were permeabilized with 0.8% TrionX-100 followed by incubation in 10% serum blocking buffer for at least 1 hour at room temperature. Primary antibody incubation overnight at 4°C was followed by secondary antibody incubation for 2 hours at room temperature. Confocal z-stack images were obtained using Fluoview1000 (Olympus), projected using National Institutes of Health (NIH) ImageJ and further processed using Inkscape. Antibodies used in this study and their dilution were as followed: Alexa488-conjugated mouse anti-Tuj1 (1:300; Covance), rabbit anti-Parvalbumin (PV) (1:300; Swant), rabbit anti-EphA7 (1:500; Abgent), goat anti-EphA7 (1:300; R&D), mouse anti-CtBP2 (1:300; BD Transduction Laboratories).

In situ hybridization

In situ hybridization was performed as previously described (Wang et al., 2013). Probes were generated using cDNA probes by RT-PCR. Primer pair for EphA7 follows: forward 5'-ATGAGGCTTAAGACTGCAGGAG-3' and reverse 5'-

CAGACGAAGCTCAGCCTTTTAT-3'. After subcloning, the identity of the probe was confirmed by DNA sequencing.

Cochlea and SGN explant culture

C57BL/6 mice were euthanized according to the *National Institutes of Health Guide for the Care and Use of Laboratory Animals*. Cochlear epithelium with SGNs attached was removed mechanically from the bone structure in Leibovitz's L-15 medium (Invitrogen). For whole-mount explant culture, the dissected cochlea was place on a Cell-Tak Cell and Tissue Adhesive (BD Biosciences) pre-coated 10 mm culture dish and cultured in DMEM/F12 supplemented with 10% FBS, 1% N2 supplement and 0.3 mg/ml ampicillin. For 5-Iodotubercidin experiments, 5-Iodotubercidin (10 μM; Tocris) was added in the explant culture after being cultured for 4 hours, and then the culture was maintained for 48 hours in a humidified atmosphere with 5% CO_2/95% air. For SGN cultures, the dissected cochlear epithelium was further microdissected to isolate a piece of SG. For consistency, exactly one turn away from the apex of a cochlea was set as the starting point of dissection. Once the SG was isolated, pieces were cut in a comparable length and placed on a layer of solidified Matrigel (BD Biosciences). Then, another layer of Matrigel was added and the dish was incubated at 37°C. After a complete solidification of the Matrigel, cochlear medium was added and explants were allowed to grow for 12 hours. Chemical inhibitors/stimulators, either 3μM 5-Iodotubercidin (in DMSO), 0.5μM FR180204 (in DMSO), 1mM 8-Bromo-cGMP (in water) or DMSO alone (as control), were then added and cultured for 24–48 hours. For siRNA experiments, dissected SG was placed in either standard control siRNA (Santa Cruz Biotechnology) or EphA7-specific siRNA (Santa Cruz Biotechnology) drops diluted with PBS on a Sylgard-coated dish and then electroporated using a custom-made electroporator. Sample was further cultured in 3D Matrigel for 4 days.

TMRD labeling

Mouse inner ear bone with intact auditory nerve projecting out from the bone structure, was dissected out in the artificial cerebrospinal fluid (ACSF). A small piece of TMRD crystal was applied to the auditory nerve outside of the bone structure and incubated for 30 minutes at room temperature. The bone structure was washed with ACSF for several times and incubated in oxygenated ACSF for at least 4 hours at room temperature. Cochlea was then dissected out and washed extensively with ACSF and fixed with 4% PFA overnight.

Western blot

Proteins of cultured SGs were extracted using Qproteome Mammalian Protein Prep Kit (Qiagen) and stored at −80°C with 20% glycerol. Boiled protein extracts were separated with NuPAGE Novex Bis-Tris gel (Invitrogen) and transferred using Trans-Blot Turbo Transfer System (Bio-Rad). Extracts were probed with anti-EphA7 antibody (1:500; R&D) or anti-β-tubulin (1:1000; Cell Signaling), followed by secondary antibody incubation with peroxidase-conjugated IgG (Jackson Immunoresearch).

Image analysis and quantification

All the confocal image stacks were processed in Fiji (ImageJ) software. For calculating area occupancy by inner radial bundles, whole-mount immunostained z-stacked images were converted to binary images. Pixels of outlined objects in binary images were then counted and subtracted from the pixel number of the total area. The measured total area extended from the SG boundary to the inner hair cell layer. Significance was tested using two-tailed Student's t-test for two group comparisons, or one-way ANOVA followed by Tamhane's T2 post hoc test for multiple group comparisons.

To quantify the number of inner radial bundle trunks, an image layer from the z-stacked image acquired at 40X magnification, representing the most medial part of the inner radial bundle growing out from SGN somas, was chosen for counting the number of bundles. Branches emerging from the middle of inner radial bundles or branches crossing to other bundles were not counted. The average bundle thickness (i.e. mean bundle width) was calculated by dividing the total length of space occupied by inner radial bundles (at the same plane as described above) by the number of bundles (Wang et al., 2013). To quantify the number of small fascicles per inner radial bundle, the total number of fascicles at 10 μm distance medially from the inner hair cell layer was counted, and the number was then divided by the number of inner radial bundles in the chosen area. Significance was tested using two-tailed Student's t-test.

Tuj-1 and DAPI immunostained whole-mount and 20μm cross-sectional P8 cochlear images were used to manually count SGN somas in a chosen area. To quantify ribbon synapses of inner hair cells, whole-mount cochleae stained with anti-CtBP2 were used. For counting ribbon synapses on outer hair cells, confocal z-stacked cross-sectional images at 5 μm intervals were used. The total number of ribbon synapses was divided by the total number of HC nuclei to obtain the average number of synapses per HC. Significance was tested using two-tailed Student's t-test.

For measuring neurite length in *in vitro* explants, distance from the somata boundary to the distal end of the neurite was measured. The number of outgrowing neurites, i.e. neurites that directly projected out from SGN somas, were manually counted. Staining procedures and image setting were identical for all samples in the same experiments for comparison. Significance was tested using Wilcoxon rank-sum test.

Auditory brainstem response (ABR) recording

5-week old mice were anesthetized with ketamine (80mg/kg) and xylazine (10mg/kg) mixture. The body temperature was maintained at 37°C with a heating pad and a rectal probe. ABRs were evoked by tone bursts (5-ms duration, with 0.5-ms rise-fall time) at frequencies of 8, 12, 16, 24, 32 kHz. The tone intensity was increased in 5 dB steps from 10 dB to 100 dB sound pressure level (SPL). Responses at each frequency and intensity level, averaged across 1000 repetitions, were acquired using EPL Cochlear Function Test Suite (Massachusetts Eye and Ear) (Niu et al., 2006). Threshold was identified by visual inspection of waveforms.

RESULTS

EphA7 is a candidate factor for regulating SGN development

To identify genes that might play a role in cochlear development, we performed RNA-sequencing to screen for genes that are differentially expressed in sensory epithelial cells in the organ of Corti (OC) and non-sensory-epithelial cells. Non-sensory-epithelial cells we sampled included cells in the GER and SG, while sensory epithelial cells consisted of both inner and outer hair cells (IHC and OHC respectively). We took advantage of available transgenic mouse lines where different cell types were labelled genetically. As we previously reported (Wang et al., 2013), in the Parvalbumin (PV)-Cre line, Cre activity in the cochlea was limited to HCs and SGNs, as shown by the green fluorescence pattern in the PV-Cre mouse crossed with a Cre-dependent reporter line, Ai6 (zsGreen) (Fig. 1A,B). The fluorescence labelled HC layers and SG were surgically separated. In the Gad1-GFP line, green fluorescence was specifically observed in cells in the GER region (Fig. 1C,D). From dissociated cell samples at ages between postnatal day 3 (P3) and P7, we purified HCs, SGNs and GER cells through fluorescence-activated cell sorting (FACS) as described previously (Wang et al., 2013) (see Methods). RNA sequencing analysis was then performed. We found that various established cell markers for HCs and GER cells were highly enriched in the correspondingly designated samples (Fig. 1E), verifying the purity of the isolated cell groups. Parvalbumin (“Pvalb”) and Gad1, the restricted expressions of which formed the basis for our cell sorting, were also confirmed to be highly enriched in the expected cell samples (Fig. 1E).

In this study, we focused on Eph/ephrin signaling pathways, as they have previously been shown to affect the formation of neural circuitry in the auditory pathway (Coate et al., 2012; Defourny et al., 2013; Ilona et al., 2007). From the expression pattern of ephrin type A receptors, EphA7 and EphA4 stood out as top candidate factors for regulating SGN development (Fig. 1F). Since EphA4 signalling has been shown to be involved in fasciculation of radial fibers and targeting of type I fibers to the IHC layer (Coate et al., 2012; Defourny et al., 2013), we hypothesized that EphA7 might act as an additional factor for regulating the development of HC innervation pattern.

To verify the expression of EphA7 gene in the mouse cochlea, we performed *in situ* hybridization in the whole-mount cochlea (Fig. 2A,B) and cochlear cross sections (Fig. 2C–E). At P3, relatively strong EphA7 signals were found in the SG and GER regions (Fig. 2A–E). Within the SG, there were patches of cells that appeared to lack or have very weak EphA7 expression (Fig. 2B,D), suggesting that not all SGNs expressed EphA7. The cross-sectional view also revealed a strong expression of EphA7 transcripts in the OC and the lesser epithelial ridge (LER) (Fig. 2E). Immunostaining of the cochlea at the same age with an anti-EphA7 antibody showed an expression pattern of EphA7 proteins similar to EphA7 transcripts: EphA7 proteins were strongly expressed in the SG, GER and OC regions (Fig. 2H–K). Weaker signals were also observed in the otic mesenchyme (OM), indicating that EphA7 proteins were also expressed in at least some mesenchymal cells (Fig. 2H–K). The overall expression pattern of EphA7 transcripts at E14.5 was largely consistent with that at P3: the expression was strong in the SG and GER regions, and was also observed in the OC

(Fig. 2F–G). Finally, high magnification images of immunostaining confirmed that some SGNs lacked expression of EphA7 (Fig. 2L–N). Together, our data suggest that EphA7 is not only differentially expressed in the population of SGNs, but also is expressed in many other cell populations in the surrounding regions such as the OM, GER and OC. These *in situ* and immunostaining data are largely in agreement with our RNA-sequencing data at postnatal stages and with a previous study of EphA7 expression in the mouse cochlea (see Shared Harvard Inner-Ear Laboratory Database, http://shield.hms.harvard.edu/).

SGN fiber bundles are sparser when EphA7 is lost

Since EphA7 has previously been shown to promote neurite outgrowth and growth cone spreading in chick spinal motor neurons (Marquardt et al., 2005), we hypothesized that SGNs might require EphA7 for the proper growth and maintenance of their axons. To test this possibility, we examined the HC innervation pattern of SGN fibers in the whole-mount cochlea, by immunostaining with an anti-Tuj1 antibody. At E18.5, SGN fibers appeared densely packed and formed well-organized inner radial bundles along the length of the cochlea in both the wild-type and EphA7 mutant animals (Fig. 3A–C). Higher-magnification images however revealed that inner radial bundles were noticeably sparser in EphA7 homozygous than heterozygous mutants (Fig. 3D–E) and wild-type animals (images not shown). We then examined SGN fibers at different time points during development. At E16.5, inner radial bundles in the EphA7−/− cochlea already appeared sparser as compared with heterozygous and wild-type animals, especially in the base and mid part of the cochlea (Fig. 3F–N). Such differences were observed throughout the developmental periods as late as P8 (Fig. 3O–T), when all HCs are innervated by SGN fibers and become synaptically matured (Lu et al., 2011).

To quantify the sparseness of inner radial bundles, we measured the total area of space between the SG and sensory epithelium that was not occupied by SGN fibers. As shown by the black-and-white binary images (Fig. 4A,B), the unoccupied/vacant space was evidently larger in EphA7 homozygous than heterozygous mutants. The quantification confirmed that inner radial bundles in EphA7−/− mutants consumed less space compared with wild-type and heterozygous animals, and these differences were evident throughout the developmental periods from E16.5 to P8 (Fig. 4C). Wild-type and EphA7+/− animals did not have significant differences from each other (Fig. 4C).

The increase in the vacant space in EphA7−/− mutants could not be simply attributed to a fasciculation effect as there was no significant difference in average radial bundle thickness between genotypes (mean bundle width: 26.1 ± 0.95 μm for homozygous and 25.3 ± 0.83 μm for heterozygous at E16-E18, $p = 0.55$, t test; see Methods). Neither could the increase be attributed to a difference in cochlear size (see Fig. 3A–C). On the other hand, the number of inner radial bundles was significantly reduced throughout the developmental periods when EphA7 was absent (Fig. 4F,G,I). In addition, the average number of small fascicles in the inner spiral plexus (ISP, medial to the IHC layer) per inner radial bundle (trunk) was significantly reduced in EphA7−/− mutants after birth (Fig. 4D,E,H), indicating that the total number of small fascicles of SGN fiber entering the OC was reduced across the

developmental stages examined. Together, our data suggest that the loss of EphA7 causes a reduced number of SGN fibers.

Sparser type I afferent fibers lead to a reduced number of ribbon synapses

Previously it has been shown that EphA7 regulates apoptosis of forebrain neural progenitors (Depaepe et al., 2005). The apparent reduction in the number of radial bundles led us to suspect that EphA7 deletion might cause a loss of SGNs. To test this possibility, we counted SGNs, immunostained with anti-Tuj1 and DAPI (Fig. 5A,B). We did not however find a difference in the total number of SGNs between EphA7−/− and EphA7+/− littermates (Fig. 5C), indicating that the observed reduction of HC-innervating fibers was not due to reduced SGN cell number. We next examined whether the reduction in fiber density led to a change in synapse number on HCs. Using an anti-RIBEYE/Ctbp2 antibody, we quantified the mean number of ribbon synapses on individual IHCs and OHCs (Fig. 5D–G). For OHCs, cross-sectioned tissues were used for better resolving synaptic puncta at the base of OHCs (Fig. 5F,G). In P8 tissues, we found fewer synaptic puncta on IHCs in EphA7−/− than EphA7+/− mutants, whereas no significant difference in synapse number was observed for OHCs (Fig. 5H).

SGNs are subdivided into two classes: type I (90% of the entire SGN population), whose fibers form synapses on IHCs, and type II (the remaining 10% of the SGN population), whose fibers grow past the IHC layer, and then turn before forming synapses on OHCs (Huang et al., 2007; Koundakjian et al., 2007). The reduction of synapse number on IHCs implied that the number of type I afferent fibers might be specifically reduced by deletion of EphA7. To confirm this notion, we specifically labelled type I fibers with tetramethylrhodamine-conjugated dextran (TMRD) (Huang et al., 2007). Consistent with the result on labelling of all types of fiber, we found a clear reduction of type I fiber innervation in EphA7−/− mutants, as evidenced by a lower number of small fascicles in the ISP compared with EphA7+/− littermates (Fig. 5I–K). It is worth noting that the TMRD labelling in the OHC layers at this stage (P4) is consistent with previous results showing transient innervation of the OHC layers by type I fibers during early development before they are completely withdrawn from the OHC layers at P6 (Perkins and Morest, 1975; Huang et al., 2007). The combined anatomical evidence indicates that the loss of EphA7 leads to a reduction in the number of type I SGN fibers, resulting in diminished synapse numbers specifically on IHCs.

EphA7 influences the outgrowth of SGN neurites

Previous studies have implicated Eph/ephrin signalling in regulating the branching and growth dynamics of neuronal processes (Benson et al., 2005; Brownlee et al., 2000; Gao et al., 2000; Wang et al., 1997; Zhou et al., 2001). The *in vivo* result of less dense SGN fibers suggests that EphA7 may be involved in regulating the outgrowth of SGN neurites. To test this possibility, we cultured isolated SG explants from E16.5 EphA7−/− and heterozygous littermates in Matrigel for 4 days (Fig. 6A,B). While there was no difference in tissue size between EphA7−/− and EphA7+/− explants (explant diameter: 177 ± 30 μm and 168 ± 20 μm respectively, $p > 0.05$, t test), the homozygous explants extended fewer neurites compared with the heterozygous explants (Fig. 6C). The mean neurite length was also

shorter in homozygous than heterozygous explants (Fig. 6D). These results suggest that the development of SGN fibers is altered in a cell-type autonomous (i.e. interactions occur between cells of the same type) manner when the endogenous EphA7 signalling is interrupted.

To further confirm the role of EphA7 in regulating the number of SGN neurites, we applied another loss-of-function approach by RNA interference. We identified a target-specific siRNA against EphA7, which effect of reducing EphA7 translation was validated by western blot (Fig. 6E). We electroporated the EphA7 siRNA or a control scrambled siRNA into wild-type SG explants (see Methods). After 4 days in culture, we found that EphA7 knockdown impeded neurite outgrowth from SGN somata, as evidenced by the greatly reduced number of neurites as compared with the control siRNA (Fig. 6F–H). It is noticeable that the procedure of siRNA electroporation *per se* had some effect on neurite growth, so that there was a general reduction of neurite number (compare heterozygous control in Fig. 6C with control siRNA in Fig. 6H, or homozygous mutant in Fig. 6C with EphA7 siRNA in Fig. 6H). The relative reduction of neurite number is 38% in the case of EphA7 knockout (Fig 6C), while 25% in the case of EphA7 knockdown (Fig 6H). Therefore, although any off-target effects could not be excluded, the EphA7 siRNA essentially produced a similar effect as the EphA7 knockout. For the few neurites that had projected from SGN somata, their lengths were significantly reduced compared with tissue treated with the control siRNA (Fig. 6I). This difference could not be explained by differential cell death since there was no significant difference in explant size after electroporation and culturing between EphA7 siRNA and control siRNA groups (diameter: 253.3 ± 50.9 μm and 251.3 ± 61.7 μm, respectively, $p = 0.97$, t test). Furthermore, we treated SG explants with an unclustered, soluble form of EphA7-Fc, which can act as a blocker of endogenous EphA7 signalling, since it competes with endogenous EphA7 receptors for ligands (Davis et al., 1994). Compared with control IgG-Fc, the unclustered EphA7-Fc applied exogenously reduced the number of neurites extended from SGN somata (Fig. 6J). Together, these *in vitro* results further demonstrate that the absence of EphA7 signalling leads to a reduced number of SGN neurites. In addition, the results suggest that the natural ligands for EphA7 receptors may be expressed by SGNs themselves.

Loss of EphA7 affects synaptic transmission at the IHC afferent synapse

To examine the effect of reduced synaptic contacts on IHCs at a functional level, we measured the auditory brainstem response (ABR) evoked by short tone bursts. Although there was no significant difference in hearing thresholds between genotypes (EphA7+/−: 25 ± 2 dB SPL; EphA7−/−: 37 ± 4 dB SPL, $p > 0.05$, t test), analysis of the first peak of the ABR waveform (i.e. peak I), which reflects the summed activity of SGNs (Melcher et al., 1996), showed a decrease in its amplitude in EphA7−/− mutants as compared with heterozygous littermates (Fig. 7A). The decrease in peak I amplitude was significant at high sound intensities (70–90 dB SPL) (Fig. 7B). The amplitudes of later peaks of the ABR waveform were also reduced but to a lesser extent (Fig. 7C). These results suggest that the reduction of IHC afferent synapses in EphA7−/− mutants is significant enough to cause decreased SGN response activity, but the defect is eventually compensated to some extent along the ascending central auditory pathway.

ERK activity may be involved in SGN neurite development

A previous study has reported that EphA7 activation is accompanied by phosphorylation of extracellular-signal regulated kinase 1/2 (ERK1/2) (Nakanishi et al., 2007). Here, we sought to inhibit ERK1/2 phosphorylation by applying a known ERK phosphorylation inhibitor, 5-Iodotubercidin (5-ITU) (Browning et al., 2005; Gambelli et al., 2004; Nakanishi et al., 2007). Treatment of E17.5 whole-mount cochleae with 5-ITU for 2 days resulted in diminished SGN fibers and a great loss of small fascicles in the ISP region (Fig. 8A,B), as demonstrated by the significantly larger vacant space as compared with explants treated with the control vehicle (Fig. 8C). In cultured SG explants incubated with 5-ITU, we also observed a reduction in the number of neurites (Fig. 8D,E,G). Furthermore, incubation of explants with FR180204, a selective inhibitor of the kinase activity of ERK1/2 (Ohori et al., 2005), resulted in a drastic reduction in the number of neurites (Fig. 8F,G), further suggesting that ERK1/2 activity is important for the initial growth of SGN neurites.

Previous studies have reported that cGMP-dependent protein kinase 1 (Prkg1) is expressed in SGNs and that it can modulate ERK1/2 activity (Jaumann et al., 2012; Komalavilas et al., 1999). We further examined SGN innervation patterns in Prkg1 knockout mice. Since these animals were embryonic lethal, all the experiments were carried out at embryonic stages. Prkg1−/− phenotype resembled that of EphA7−/− mutants, with the defect apparently to a more severe degree (Fig. 9A–F). There was a significant reduction in the number of inner radial bundles and increase in the area of space unoccupied by SGN fibers in Prkg1−/− mutants as compared with wild-type animals (Fig. 9G,H). While the average number of small fascicles per inner radial bundle was not significantly different between Prkg1−/− and wild-type animals (Fig. 9I), the reduced number of inner radial bundles (Fig. 9H) indicated a reduction in the total number of small fascicles. The number of SGN somata was not different between the Prkg1 knockout and its wild-type control at E17.5 (Fig. 9J–L), excluding the possibility of increased cell death. We further tested the effect of Prkg1 activity *in vitro*, by applying 8-Br-cGMP, an activator of Prkg1. Treatment of wild-type SG explants with 8-Br-cGMP resulted in a large increase in the number of neurites at 16 hours after treatment as compared with the control vehicle (Supporting Information Fig. 1A–C), suggesting that enhancing Prkg1 activity can promote neurite growth. Furthermore, in EphA7−/− explants, 8-Br-cGMP treatment also resulted in enhanced neurite growth (Supporting Information Fig. 1D–F), suggesting that enhancing Prkg1 activity may overturn the defect of EphA7 deletion. These results further support a potential involvement of ERK1/2 in EphA7 signalling.

DISCUSSION

Eph signaling pathways are known to be key modulators in neural development. Their unique functions in cochlear development however are only beginning to be explored. Our study reveals a molecular component in these pathways important for cochlear patterning. Based on the genetic and functional analyses, we conclude that EphA7 plays an important role in regulating the development of SGN neurites.

Regulation of axonal growth by EphA7

Multiple roles of EphA7 in the assembly of neural circuitry have been characterized. In mouse cortical neurons, EphA7 mediates dendritic growth, dendritic spine formation, synaptic maturation (Clifford et al., 2014), and organization of a topography of corticothalamic projections (Torrii and Levitt, 2005). During development of retinocollicular projections, EphA7 is invovled as a repellent substrate for directing retinal axon pathfinding (Rashid et al., 2005). Furthermore, it is implicated in controling apotosis of forebrain neural progenitors (Depaepe et al., 2005). Having such multiplex functions is not uncommon for Eph and ephrin family molecules, as other axon guidance molecules, such as netrin, can also act as a chemoattractant or chemorepellant depending on the type of axons (Serafini et al., 1994; Colamarino and Tessier-Lavigne, 1995). Here, we demonstrate that EphA7 signaling in the mouse cochlea is important for the initial growth of SGN processes. Previous evidence of EphA7 promoting axonal outgrowth through reverse signaling (Chai et al., 2014; Lewcoc et al., 2007) suggests that signaling via EphA7 in SGNs may also play a unique role in modulating their axonal outgrowth, thereby controlling the number of type I fibers innervating IHCs. While Eph receptors are generally thought to have a repulsive/negative effect on neuronal growth or migration, our data suggest that they can also have a stimulative/positive effect on neurite growth. This is reminiscent of several *in vitro* studies showing that ephrins can either stimulate or inhibit neurite outgrowth depending on different developing systems and possibly also different stages of neurons (Gao et al., 2000; Zhou et al., 2001). Alternatively, EphA7 may play a permissive role, and removing EphA7 activity therefore impedes the normal neurite outgrowth.

Potential ligands for EphA7 signaling

Previously EphA4 has been shown to exert both a cell-autonomous and non-cell-autonomous function in the formation of axon tracts (Dottori et al., 1998; Kullander et al., 2001; Marquardt et al., 2005). For the latter, the kinase activity of EphA4 is not required, suggesting that EphA4 acts as a ligand. In this study, our *in vitro* explant experiments demonstrated that EphA7 signaling in SGNs is activated independent of mesenchymal cells surrounding the SG. In addition, the number of SGN neurites is reduced in isolated SG explants treated with unclustered EphA7-Fc, which competitively binds to EphA7-interacting ligands and blocks endogenous EphA7 signaling. These results indicate that EphA7-interacting ephrins are expressed in SGNs themselves. Previously it has been shown that EphA7 reverse signaling plays a role in promoting motor neuron axon outgrowth (Chai et al., 2014). There are also studies showing that forward signaling can stimulate axon outgrowth (Hansen et al., 2004; Lewcock et al., 2007). Considering that Eph and ephrine molecules are likely spatially segragated from each other on the membrane of the parent cell (Marquardt et al., 2005), we postulate that both reverse and forward EphA7 signalling activated by interactions between EphA7 and its ligands on neighouring SGNs may play a role in regulating SGN neurite growth.

What are possible ligands for EphA7 then? Based on the partially overlapping expression patterns of EphA7 and ephrin-A5 in type I SGNs (our unpublished data) and the previous evidence implicating EphA7/ephrin-A5 interactions (Gale et al., 1996; Clifford et al., 2014), it is possible that EphA7 signaling is achieved through ephrin-A5 binding. Although there

are studies showing that suppression of ERK activity by ephrin-A5 caused a growth cone collapse in retinal ganglion cells, hippocampal neurons and SGNs (Defourny et al., 2013; Drescher et al.,1995; Meier et al., 2011), in these experiments ephrin-A5 was applied for only a breif period of time (15–60 min). Prolonged exposure of ephrin-A5 in fact induces expression of cytoskeletal genes such as actinin (Meier et al., 2011), suggesting that it can play a role in promoting axonal growth. The exact time lapse from initial cell-cell contact to a complete morphological change due to Eph/ephrin interactions is not known in *in vivo* conditions, but a continuous expression of EphA7 and ephrin-A5 in developing SGNs during the entire processes of neurite outgrowth and formation of synaptic connections suggests a long-term interaction of the two molecules under physiological conditions. Other potential ligands that might be involved in reverse signaling could be ephrin-A2 and ephrin-B2. The interaction between EphA7 and ephrin-A2 in reverse signaling has been previously established in the adult mouse brain. This interaction negatively regulates the proliferation of neural progenitor cells, as neurogenesis in the olfactory bulb is increased in mice lacking ephrin-A2 (Holmberg et al., 2005). Furthermore, a gradient expression of ephrin-A2 in the SG (Lee and Warchol, 2005) makes it an interesting EphA7 partner as topographic mapping is established in a concentration-dependent manner (Hansen et al., 2004). Ephrin-B2 is also highly expressed in SGNs (Coate el al., 2012). Although the binding of ephrin-B2 to EphA7 needs to be validated with biochemical experiments, a previous study suggests that ephrin-B2 mediated reverse signaling via EphA7 is responsible for the development of nephric duct (Weiss et al, 2014), raising the possibility of ephrin-B2 being an EphA7-ineracting partner in the SG as well. More extensive investigations are needed to fully identify the EphA7 ligands.

As multiple ephrin family members are present throughout the cochlear development, it is possible that there is a functional redunduncy among these members and that the effect of EphA7 knockout can be compensated to some extent by upregulating other Eph/ephrin signaling mechanisms. Indeed, there are various studies suggesting compensatory mechanisms of Eph/ephrin signaling during neural development (Feldheim et al., 2000; Lim et al., 2008; Orioli et al., 1996; Passante et al., 2008). Considering the diversity of the biological processes influenced by Eph/ephrin signaling, it is interesting to note that most of ephrin type-A receptor knockout mice are viable, likely due to compensation effects. In the present study, we observed a more pronounced effect of reducing SGN neruites by blocking downstream signaling molecules (e.g. with FR180204) than knocking down EphA7, which is consistent with potential compensatory effects caused by increased expression of other Eph molecules when EphA7 is absent.

Other potential effects of EphA7 in cochlear development

Several lines of evidence suggest a stage-dependent role of EphA7 in the morphological development of cortical and hippocampal neurons (Clifford et al., 2014; Zhou et al., 2001). In the mouse cochlea, the effect of EphA7 in regulating neurite outgrowth also seems neuronal stage dependent. Early embryonic SG explants were responsive to unclustered EphA7-Fc, while postnatal explants did not show a significant change in neurite number under treatment of unclustered EphA7-Fc (data not shown). Since SGNs, initially derived from the neuroblasts from the otocyst, become postmitotic around E11.5 to E15.5, it rasies

the possibility that postmitotic neurons may gradually lose the responsiveness to EphA7 activation.

It is well known that several axon guidance molecules are present in non-sensory regions of the cochlea such as the GER and mesenchyme. They may play a regulatory role in SGN migration and in the proper organization and guidance of neurite extension, as have been shown previously (Bianchi and Liu, 1999; Coate et al., 2012; Wang et al., 2013). Our gene expression and immunohistochemistry studies showed that EphA7 is also expressed in the GER and mesenchymal cells. The role of EphA7 molecule in these cell populations is unclear, as there is no obvious defect in axon fasciculation or pathfinding in the EphA7 knockout mouse. Considering the fact that other ephrin signaling pathways such as those via EphB2 can influence non-neuronal cell populations in the ear (Cowan et al., 2000), different roles of EphA7 in other regions are plausible. In fact, potential influence of EphA7 on non-neuronal populations in the developing mouse ear has been implicated before. For example, a strong expression of EphA7 in the invaginating otic cup starting around E8.5 suggests an involvement of EphA7 in the otic development concerning border distinction around the otic cup or its invagination process (Saeger et al., 2011).

Signaling of EphA7

The challenge in assembling Eph/ephrin signaling pathways is that various cross-talks may occur with each other and with other signaling cascades to achieve biological goals (Arvanitis and Davy, 2008; Klein, 2004). Recent data have linked Eph receptor signaling to the Ras and Rho protein families. EphA7 activation is implicated in regulating Ras, which eventually activates a casade of kinases such as ERK1 and ERK2 (Nakanishi et al., 2007). Although much of the investigation into EphA7 signaling pathways has been carried out in cancer cells associated with leukemia and lymphoma (Nakanishi et al., 2007; Oricchio et al., 2011), it is possible that the signaling pathways in different cell types may share common mediators. Additionally, ephrin-A mediated reverse signaling has also been shown to activate ERK pathways (Davy et al., 1999). Our results presented in this study show that inhibition of ERK1/2 phosphrylation and kinase activity *in vitro* and *ex vivo* produces a similar effect of reducing SGN fibers as in EphA7 deletion mutants, suggesting a possible involvement of ERK1/2 activity in EphA7 signaling during SGN development. Furthermore, previous studies demonstrating an initiation of cytoskeletal interactions upon ERK1/2 activation (Forcet et al., 2002; Veeranna et al., 1998; Wang and Hatton, 2007), which is essential for neurite outgrowth, further complement our results.

Functional relevance of EphA7 signaling

Hearing loss can severely impair an important aspect of everyday life, leading to a dramatic reduction in quality of life. Our data indicate that EphA7 deletion does not simply cause a hearing loss. However, a significant decrease in the amplitude of peak I of ABR, which reflects summed activity of SGN fibers, only at high sound intensities suggests that the defect may reflect a form of hidden hearing loss (Schaette and McAlpine, 2011). In hidden hearing loss, the unresponsiveness to sound in a fraction of auditory nerve fibers, possibly the ones having high thresholds and low spontaneous rates and thought to be involved in encoding high-intensity acoustic information (Young and Barta, 1986), leads to an increased

response gain in the auditory brainstem. This can result in normal or minimally reduced peak V amplitudes (Schaette and McAlpine, 2011). Such compensatory increase in response gain may lead to tinnitus due to enhancement of spontaneous activity of auditory neurons (Schaette and McAlpine, 2011). In our ABR data, we do observe changes of peak I and peak V amplitudes consistent with hidden heaing loss. Although caution has to be taken before intepretating our data as an indication of hidden hearing loss and tinnitus, it is possible that deafferentation of auditory nerve fibers caused by mutations of EphA7 can contribute to the hearing disorders.

The function roles of Eph/ephrin family molecules in the cochlea are beginning to be unveiled. Future studies with spatially and temporally controlled knockouts of Eph and ephrin members will provide a deeper understanding of Eph/ephrin signaling in the developing cochlea.

Supplementary Material

Refer to Web version on PubMed Central for supplementary material.

Acknowledgement

This work was supported by grants to L.I.Z. from the US National Institutes of Health (DC008983) and the David and Lucile Packard Foundation. H.W.T was supported by a grant from the US National Institutes of Health (R01EY019049). W.Y. was supported by grants from the National Natural Science Foundation of China (NSFC: 30973301, 81271080, 81470694). We thank Drs. M. Coba and J. Li for the help on western blot.

REFERENCE

Arvanitis D, Davy A. Eph/ephrin signaling: networks. Genes Dev. 2008; 22:416–429. [PubMed: 18281458]

Benson MD, Romero MI, Lush ME, Lu QR, Henkemeyer M, Parada LF. Ephrin-B3 is a myelin-based inhibitor of neurite outgrowth. Proc Natl Acad Sci USA. 2005; 102:10694–10699. [PubMed: 16020529]

Bianchi LM, Gale NM. Distribution of Eph-related molecules in the developing and mature cochlea. Hear Res. 1998; 117:161–172. [PubMed: 9557986]

Bianchi LM, Gray NA. EphB receptors influence growth of ephrin-B1-positive statoacoustic nerve fibers. Eur J Neurosci. 2002; 16:1499–1506. [PubMed: 12405963]

Bianchi LM, Liu H. Comparison of ephrin-A ligand and EphA receptor distribution in the developing inner ear. Anat Rec. 1999; 254:127–134. [PubMed: 9892426]

Brownlee H, Gao PP, Frisen J, Dreyfus C, Zhou R, Black IB. Multiple ephrins regulate hippocampal neurite outgrowth. J Comp Neurol. 2000; 425:315–322. [PubMed: 10954848]

Chai G, Zhou L, Manto M, Helmbacher F, Clotman F, Goffinet AM, Tissir F. Celsr3 is required in motor neurons to steer their axons in the hindlimb. Nat Neurosci. 2014; 19:1171–1179. [PubMed: 25108913]

Clifford MA, Athar W, Leonard CE, Russo A, Sampognaro PJ, Van der Goes MS, Burton DA, Zhao X, Lalchandani RR, Sahin M, Vicini S, Donoghue MJ. EphA7 signaling guides cortical dendritic development and spine maturation. Proc Natl Acad Sci USA. 2014; 111:4994–4999. [PubMed: 24707048]

Coate TM, Raft S, Zhao X, Ryan AK, Crenshaw EB 3rd, Kelley MW. Otic mesenchyme cells regulate spiral ganglion axon fasciculation through a Pou3f4/EphA4 signaling pathway. Neuron. 2012; 73:49–63. [PubMed: 22243746]

Colamarino SA, Tessier-Lavigne M. The axonal chemoattractant netrin-1 is also a chemorepellent for trochlear motor axons. Cell. 1995; 81:621–629. [PubMed: 7758116]

Cowan CA, Yokoyama N, Bianchi LM, Henkemeyer M, Fritzsch B. EphB2 guides axons at the midline and is necessary for normal vestibular function. Neuron. 2000; 26:417–430. [PubMed: 10839360]

Cramer KS, Gabriele ML. Axon guidance in the audtiory system: Multiple functions of eph receptors. Neuroscience. 2014; 26:152–162. [PubMed: 25010398]

Davy A, Gale NW, Murray EW, Klinghoffer RA, Soriano P, Feuerstein C, Robbins SM. Compartmentalized signalling by GPI-anchored ephrin-A5 requires the Fyn tyrosine kinase to regulate cellular adhesion. Genes Dev. 1999; 13:3125–3135. [PubMed: 10601038]

Defourny J, Poirrier AL, Lallemend F, Mateo Sanchez S, Neef J, Vanderhaeghen P, Soriano E, Peuckert C, Kullander K, Fritzsch B, Nguyen L, Moonen G, Moser T, Malgrange B. Ephrin-A5/EphA4 signalling controls specific afferent targeting to cochlear hair cells. Nat Commun. 2013; 4:1438. [PubMed: 23385583]

Depaepe V, Suarez-Gonzalez N, Dufour A, Passante L, Gorski JA, Jones KR, Ledent C, Vanderhaeghen P. Ephrin signalling controls brain size by regulating apoptosis of neural progenitors. Nature. 2005; 435:1244–1250. [PubMed: 15902206]

Dottori M, Hartley L, Galea M, Paxinos G, Polizzotto M, Kilpatrick T, Bartlett PF, Murphy M, Köntgen F, Boyd AW. EphA4 (Sek1) receptor tyrosine kinase is required for the development of the corticospinal tract. Proc Natl Acad Sci USA. 1998; 95:13248–13253. [PubMed: 9789074]

Drescher U, Kremoser C, Handwerker C, Löschinger J, Noda M, Bonhoeffer F. In vitro guidance of retinal ganglion cell axons by RAGS, a 25 kDa tectal protein related to ligands for Eph receptor tyrosine kinases. Cell. 1995; 82:359–370. [PubMed: 7634326]

Feldheim DA, Kim YI, Bergemann AD, Frisen J, Barbacid M, Flanagan JG. Genetic analysis of ephrin-A2 and ephrin-A5 show their requirement in multiple aspects of retinocollicular mapping. Neuron. 2000; 25:563–574. [PubMed: 10774725]

Forcet C, Stein E, Pays L, Corset V, Llambi F, Tessier-Lavigne M, Mehlen P. Netrin-1-mediated axon outgrowth requires deleted in colorectal cancer-dependent MAPK activation. Nature. 2002; 417:443–447. [PubMed: 11986622]

Gale NW, Holland SJ, Valenzuela DM, Flenniken A, Pan L, Ryan TE, Henkemeyer M, Strebhardt K, Hirai H, Wilkinson DG, Pawson T, Davis S, Yancopoulos GD. Eph receptors and ligands comprise two major specificity subclasses and are reciprocally compartmentalized during embryogenesis. Neuron. 1996; 17:9–19. [PubMed: 8755474]

Gao PP, Sun CH, Zhou XF, DiCicco-Bloom E, Zhou R. Ephrins stimulate or inhibit neurite outgrowth and survival as a function of neuronal cell type. J Neurosci Res. 2000; 60:427–436. [PubMed: 10797545]

Hansen MJ, Dallal GE, Flanagen JG. Retinal axon response to ephrin-as shows a graded, concentration-dependent transition from growth promotion to inhibition. Neuron. 2004; 42:717–730. [PubMed: 15182713]

Hippenmeyer S, Vrieseling E, Sigrist M, Portmann T, Laengle C, Ladle DR, Arber S. A developmental switch in the response of DRG neurons to ETS transcription factor signaling. PLoS Biol. 2005; 3:e159. [PubMed: 15836427]

Holmberg J, Armulik A, Senti KA, Edoff K, Spalding K, Momma S, Cassidy R, Flanagan JG, Frisen J. Ephrin-A2 reverse signaling negatively regulates neural progenitor proliferation and neurogenesis. Genes Dev. 2005; 19:462–471. [PubMed: 15713841]

Holmberg J, Clarke DL, Frisén J. Regulation of repulsion versus adhesion by different splice forms of an Eph receptor. Nature. 2000; 408:203–206. [PubMed: 11089974]

Huang LC, Thorne PR, Housley GD, Montgomery JM. Spatiotemporal definition of neurite outgrowth, refinement and retraction in the developing mouse cochlea. Development. 2007; 134:2925–2933. [PubMed: 17626062]

Marquardt T, Shirasaki R, Ghosh S, Andrews SE, Carter N, Hunter T, Pfaff SL. Coexpressed EphA receptors and ephrin-A ligands mediate opposing actions on growth cone navigation from distinct membrane domains. Cell. 2005; 121:127–139. [PubMed: 15820684]

Meier C, Anastasiadou S, Knöll B. Ephrin-A5 suppresses neurotrophin evoked neuronal motility, ERK activation and gene expression. PLoS One. 2011; 6:e26089. [PubMed: 22022520]

Miko IJ, Nakamura PA, Henkemeyer M, Cramer KS. Auditory brainstem neural activation patterns are altered in EphA4- and ephrin-B2-deficient mice. J Comp Neurol. 2007; 505:669–681. [PubMed: 17948875]

Klein R. Eph/ephrin signaling in morphogenesis, neural development and plasticity. Curr Opin Cell Biol. 2004; 16:580–589. [PubMed: 15363810]

Komalavilas P, Shah PK, Jo H, Lincoln TM. Activation of mitogen-activated protein kinase pathways by cyclic GMP and cyclic GMP-dependent protein kinase in contractile vascular smooth muscle cells. J Biol Chem. 1999; 274:34301–34309. [PubMed: 10567406]

Koundakjian EJ, Appler JL, Goodrich LV. Auditory neurons make stereotyped wiring decisions before maturation of their targets. J Neurosci. 2007; 27:14078–14088. [PubMed: 18094247]

Kullander K, Mather NK, Diella F, Dottori M, Boyd AW, Klein R. Kinase-dependent and kinase-independent functions of EphA4 receptors in major axon tract formation in vivo. Neuron. 2001; 29:73–84. [PubMed: 11182082]

Lee KH, Warchol ME. Ephrin A2 may play a role in axon guidance during hair cell regeneration. Laryngoscope. 2005; 115:1021–1025. [PubMed: 15933513]

Lewcock JW, Genoud N, Lettieri K, Pfaff SL. The ubiquitin ligase Phr1 regulates axon outgrowth through modulation of microtubule dynamics. Neuron. 2007; 56:604–620. [PubMed: 18031680]

Lim BK, Matsuda N, Poo MM. Ephrin-B reverse signalling promotes structural and functional synaptic maturation in vivo. Nat Neurosci. 2008; 11:160–169. [PubMed: 18193042]

Lu CC, Appler JM, Houseman EA, Goodrich LV. Developmental profiling of spiral ganglion neurons reveals insights into auditory circuit assembly. J Neurosci. 2011; 31:10903–10918. [PubMed: 21795542]

Madisen L, Zwingman TA, Sunkin SM, Oh SW, Zariwala HA, Gu H, Ng LL, Palmiter RD, Hawrylycz MJ, Jones AR, Lein ES, Zeng H. A robust and high-throughput Cre reporting and characterization system for the whole mouse brain. Nat Neurosci. 2010; 13:133–140. [PubMed: 20023653]

Mao Y, Reiprichm S, Wegnerm M, Fritzsch B. Targeted deletion of Sox10 by Wnt1-cre defects neuronal migration and projection in the mouse inner ear. PLoS One. 2014; 9:e94580. [PubMed: 24718611]

Melcher JR, Kiang NY. Generators of the brainstem auditory evoked potential in cat. III: Identified cell populations. Hear Res. 1996; 93:52–71. [PubMed: 8735068]

Nakanishi H, Nakamura T, Canaani E, Croce CM. ALL1 fusion proteins induce deregulation of EphA7 and ERK phosphorylation in human acute leukemias. Proc Natl Acad Sci USA. 2007; 104:14442–14447. [PubMed: 17726105]

Niu H, Makmura L, Shen T, Sheth SS, Blair K, Friedman RA. Identification of two major loci that suppress hearing loss and cochlear dysmorphogenesis in Eya1bor/bor mice. Genomics. 2006; 88:302–308. [PubMed: 16488112]

Ohori M, Kinoshita T, Okubo M, Sato K, Yamazaki A, Arakawa H, Nishimura S, Inamura N, Nakjima H, Neya M, Miyake H, Fujii T. Identification of a selective ERK inhibitor and structural determination of the inhibitor-ERK2 complex. Biochem Biophys Res Commun. 2005; 336:357–363. [PubMed: 16139248]

Oricchio E, Nanjangud G, Wolfe AL, Schatz JH, Mavrakis KJ, Jiang M, Liu X, Bruno J, Heguy A, Olshen AB, Socci ND, Teruya-Feldstein J, Weis-Garcia F, Tam W, Shaknovich R, Melnick A, Himanen JP, Chaganti RS, Wendel HG. The Eph-receptor A7 is a soluble tumor suppressor for follicular lymphoma. Cell. 2011; 147:554–564. [PubMed: 22036564]

Orioli D, Henkemeyer M, Lemke G, Klein R, Pawson T. Sek4 and Nuk receptors cooperate in guidance of commuissural axons and in palate formation. EMBO J. 1996; 15:6035–6049. [PubMed: 8947026]

Pasquale EB. Eph receptor signalling casts a wide net on cell behaviour. Na. Rev Mol Cell Biol. 2005; 6:462–475.

Passante L, Gaspard N, Degraeve M, Frisen J, Kullander K, De Maertelaer V, Vanderhaeghen P. Temporal regulation of ephrin/Eph signalling is required for the spatial patterning of the mammalian striatum. Development. 2008; 135:3281–3290. [PubMed: 18755772]

Perkins RE, Morest DK. A study of cochlear innervations patterns in cats and rats with the Golgi method and Nomarkski optics. J Comp Neurol. 1975; 163:129–158. [PubMed: 1100684]

Pickles JO. Expression of Ephs and ephrins in developing mouse inner ear. Hear Res. 2003; 178:44–51. [PubMed: 12684176]

Pickles JO, Claxton C, Van Heumen WR. Complementary and layered expression of Ephs and ephrins in developing mouse inner ear. J Comp Neurol. 2002; 449:207–216. [PubMed: 12115675]

Rashid T, Upton AL, Blentic A, Ciossek T, Knöll B, Thompson ID, Drescher U. Opposing gradients of ephrin-As and EphA7 in the superior colliculus are essential for topographic mapping in the mammalian visual system. Neuron. 2005; 47:57–69. [PubMed: 15996548]

Saeger BM, Suhm M, Neubuser A. Ephrin/ephrin receptor expression during early stages of mouse inner ear development. Dev Dyn. 2011; 240:1578–1585. [PubMed: 21465626]

Schaette R, McAlpine D. Tinnitus with a normal audiogram: physiological evidence for hidden hearing loss and computational model. J Neurosci. 2011; 31:13452–13457. [PubMed: 21940438]

Serafini T, Kennedy TE, Galko MJ, Mirzayan C, Jessell TM, Tessier-Lavigne M. The netrins define a family of axon outgrowth-promoting proteins homologous to C. elegans UNC-6. Cell. 1994; 78:409–424. [PubMed: 8062384]

Tamamaki N, Yanagawa Y, Tomioka R, Miyazaki J, Obata K, Kaneko T. Green fluorescent protein expression and colocalization with calretinin, parvalbumin, and somatostatin in the GAD67-GFP knock-in mouse. J Comp Neurol. 2003; 467:60–79. [PubMed: 14574680]

Torii M, Levitt P. Dissociation of corticothalamic and thalamocortical axon targeting by an EphA7-mediated mechanism. Neuron. 2005; 48:563–575. [PubMed: 16301174]

Veeranna, Amin ND, Ahn NG, Jaffe H, Winters CA, Grant P, Pant HC. Mitogen-activated protein kinases (Erk1,2) phosphorylate Lys-Ser-Pro (KSP) repeats in neurofilament proteins NF-H and NF-M. J Neurosci. 1998; 18:4008–4021. [PubMed: 9592082]

Wang HU, Anderson DJ. Eph family transmembrane ligands can mediae repulsive guidance of trunk neural crest migration and motor axon outgrowth. Neuron. 1997; 18:383–396. [PubMed: 9115733]

Wang YF, Hatton GI. Interaction of extracellular signal-regulated protein kinase 1/2 with actin cytoskeleton in supraoptic oxytocin neurons and astrocytes: role in burst firing. J Neurosci. 2007; 27:13822–13834. [PubMed: 18077694]

Wang SZ, Ibrahim LA, Kim YJGibson DA, Leung HC, Yuan W, Zhang KK, Tao HW, Ma L, Zhang LI. Slit/Robo signaling mediates spatial positioning of spiral ganglion neurons during development of cochlear innervations. J Neurosci. 2013; 33:12242–12254. [PubMed: 23884932]

Wegener JW, Nawrath H, Wolfsgruber W, Kühbandner S, Werner C, Hofmann F, Feil R. cGMP-dependent protein kinase I mediates the negative inotropic effect of cGMP in the murine myocardium. Circ Res. 2002; 90:18–20. [PubMed: 11786513]

Weiss AC, Airik R, Bohnenpoll T, Greulich F, Foik A, Trowe MO, Rudat C, Costantini F, Adams RH, Kispert A. Nephric duct insertion requires EphA4/EphA7 signaling from pericloacal mesenchyme. Development. 2014; 141:3420–3430. [PubMed: 25139858]

Young ED, Barta PE. Rate responses of auditory nerve fibers to tones in noise near masked threshold. J Acoust Soc Am. 1986; 79:426–442. [PubMed: 3950195]

Zhou CQ, Lee J, Henkemeyer MJ, Lee KH. Disruption of ephrin B/Eph B interaction results in abnormal cochlear innervation patterns. Laryngoscope. 2011; 121:1541–1547. [PubMed: 21647913]

Zhou X, Suh J, Cerretti DP, Zhou R, DiCicco-Bloom E. Ephrins stimulate neurite outgrowth during early cortical neurogenesis. J Neurosci Res. 2001; 66:1054–1063. [PubMed: 11746437]

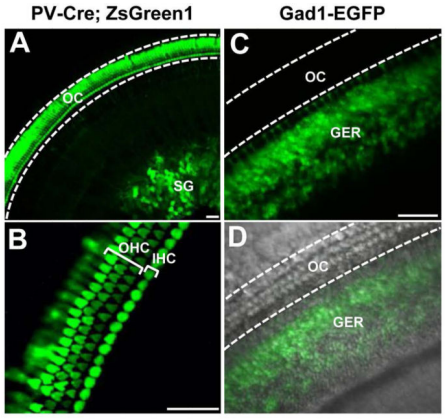

E

	Gene name	Cell type (FRKM)		
		GER	HC	SG
Hair cell specific genes	Myo6	34.17	503.17	11.85
	Chrna10	10.26	372.84	0.37
	Pvalb	15.79	311.32	56.53
	Tmc1	3.14	179.15	0.25
	Gfi1	4.01	176.90	0.00
	Otof	3.67	106.74	0.19
	Atoh1	2.32	58.35	0.18
	Pcdh15	8.72	30.09	0.72
	Barhl1	0.61	22.34	0.20
	Slc26a5	0.00	7.21	0.00
	Espn	0.57	3.53	0.00
GER specific genes	Crabp1	292.08	1.59	4.85
	Crabp2	204.63	3.08	28.26
	Jag1	118.86	6.82	7.40
	Cdh4	37.51	5.76	1.33
	Gad1	36.17	0.71	0.00

F

Gene name	Cell type (FRKM)		
	GER	HC	SG
EphA1	5.31	3.16	0.65
EphA2	0.08	0.00	0.85
EphA3	0.00	0.75	0.46
EphA4	18.45	37.08	26.35
EphA5	0.07	0.34	2.18
EphA6	0.00	0.00	0.07
EphA7	172.88	5.88	12.49
EphA8	0.00	0.00	0.19
EphA10	0.00	0.00	0.00

Figure 1.

Gene expression analysis in the mouse cochlea to identify differentially expressed ephrin type-A receptors. (A) Image of a PV-Cre::Ai6 mouse cochlea at P4. OC, organ of Corti; SG, spiral ganglion. (B) Higher-magnification image of cochlea in (A) showing HCs in the OC. OHC, outer hair cell; IHC, inner hair cell. (C) Image of a Gad1-EGFP mouse cochlea at P4. GER, greater epithelial ridge. (D) Merged differential interference contrast (DIC) and fluorescence image of the same cochlea. (E) A list of selected known HC- and GER-specific genes and their expression levels in GER, HC and SG cell samples. Numerical values are in

Fragments Per Kilobase of exon per Million (FRKM). The full names of the genes are (from top to bottom): Myo6: myosin VI; Chrna10: cholinergic receptor, nicotinic, alpha polypeptide 10; Pvalb: parvalbumin; Tmc1: transmembrane channel-like gene family 1; Gfi1: growth factor independent 1; Otof: otoferlin; Atoh1: atonal homolog 1 (Drosophila); Pcdh15: protocadherin 15; Barhl1: BarH-like 1 (Drosophila); Slc26a5: solute carrier family 26, member 5; Espn: espin; Crabp1: cellular retinoic acid binding protein I; Crabp2: cellular retinoic acid binding protein II; Jag1: jagged 1; Cdh4: cadherin 4; Gad1: glutamate decarboxylase 1. (F) A list of differentially expressed ephrin type-A receptor genes and their expression levels. All scale bars: 30 μm.

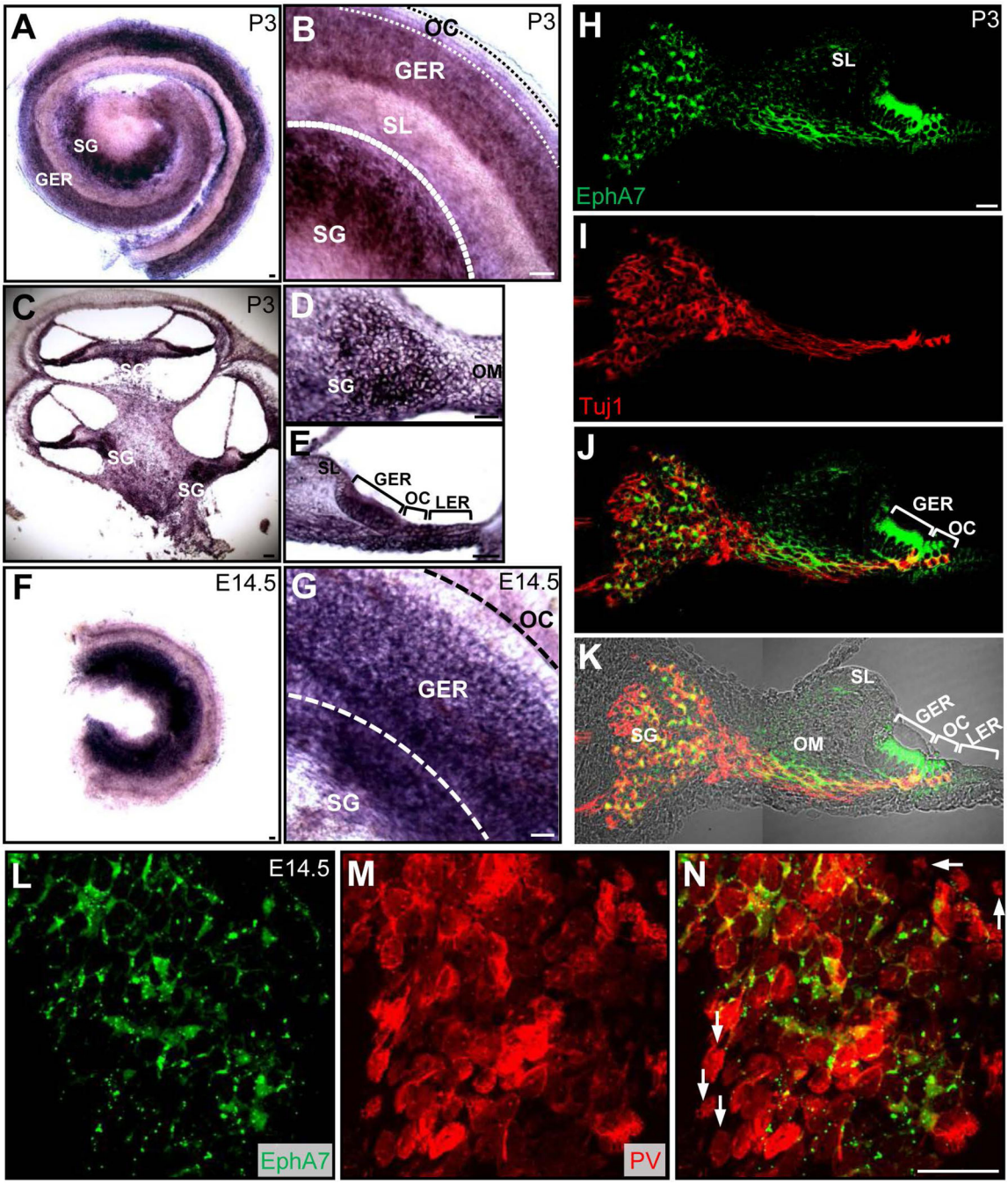

Figure 2.

Expression pattern of EphA7 in the wild-type cochlea. (A) *In situ* hybridization of EphA7 in a whole-mount cochlea at P3. SL, spiral limbus. (B) Higher-magnification image of the cochlea in (A). Different regions are labeled. (C) *In situ* hybridization of EphA7 in a cross-sectioned P3 cochlea. (D) Higher-magnification image of the SG region from (C). OM, otic mesenchyme. (E) Higher-magnification image of the sensory epithelial region from (C). LER, lesser epithelial ridge. (F) *In situ* hybridization of EphA7 in a whole-mount cochlea at E14.5. (G) Higher-magnification image of (F). Note that the SL is nearly absent at this

embryonic stage. (H–J) Fluorescence images of a cross-sectioned P3 cochlea, immunostained with anti-EphA7 (green) and anti-Tuj1 (red) antibodies. (K) Merged fluorescence (H&I) and DIC image. (L–N) High magnification images of immunostaining of SGNs with anti-EphA7 (green) and anti-PV (red) and the merged image. White arrows in (N) mark SGNs negative for EphA7 proteins. Scale bar: 100 μm in (C), 30 μm in all other panels.

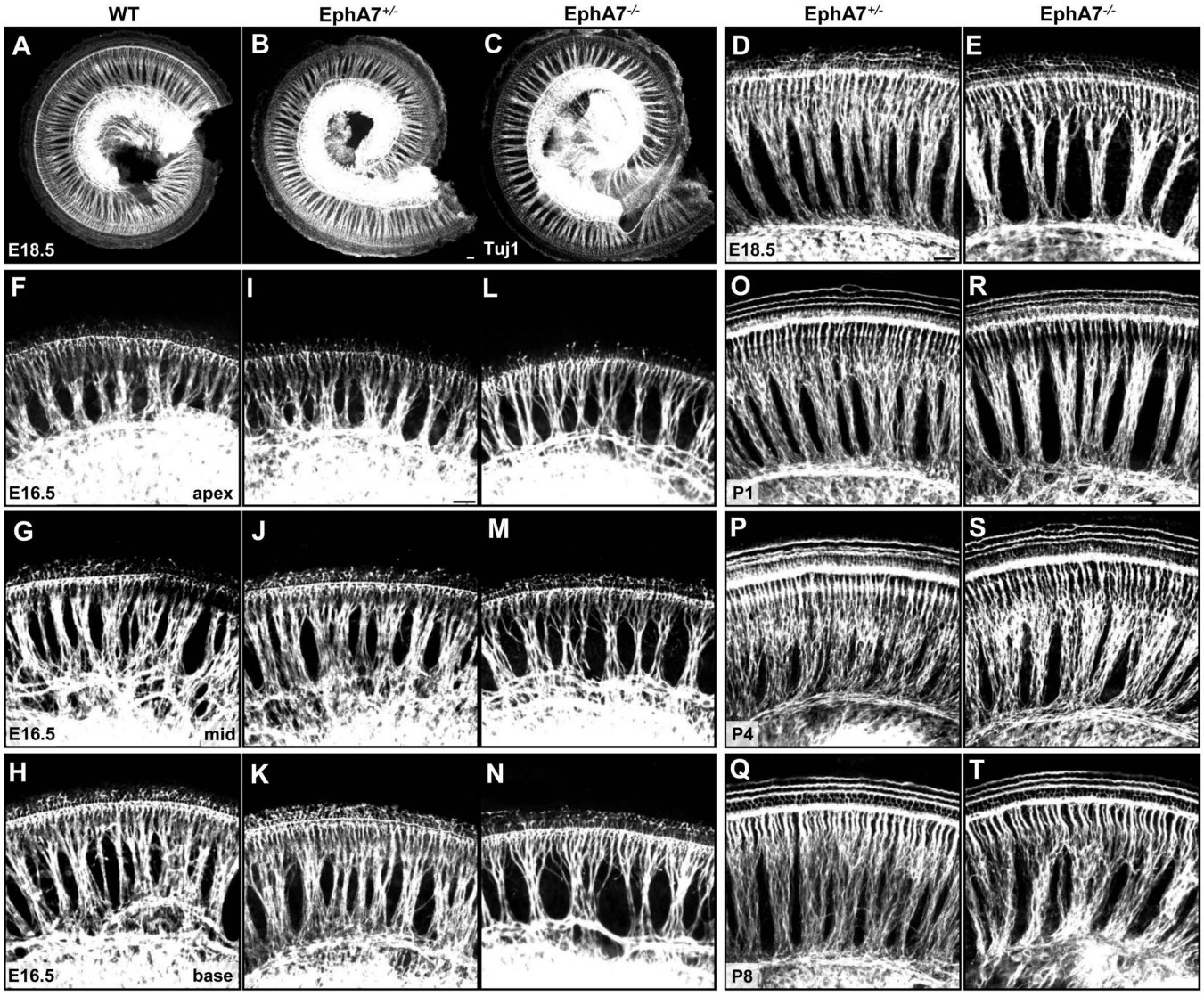

Figure 3.

Developmental changes of SGN fiber innervation pattern in EphA7 mutant cochleae. (A–C) Images of representative whole-mount cochleae from E18.5 wild-type, EphA7+/−, and EphA7−/− mice, immunostained with anti-Tuj1. (D–E) Higher-magnification images of the mid-base part of the EphA7+/− and EphA7−/− cochleae shown in (B–C). (F–N) Higher-magnification images of the apex, mid and base part of representative cochleae from E16.5 wild-type, EphA7+/−, and EphA7−/− mice, respectively. (O–T) Higher-magnification images of the mid-base part of EphA7+/− and EphA7−/− cochleae at P1, P4 and P8, respectively. All scale bars: 30 μm.

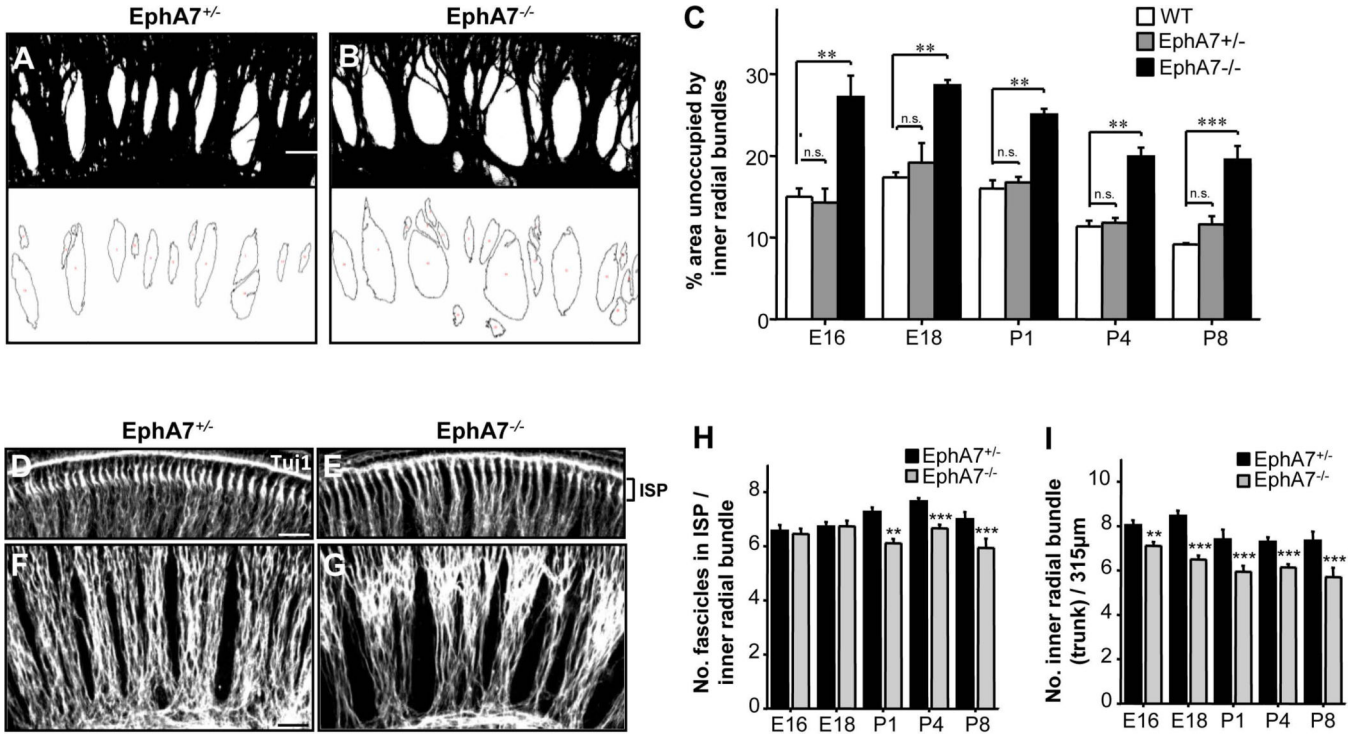

Figure 4.

Regulation of number of inner radial bundles by EphA7. (A–B) Example binary images for Tuj1-stained SGN fibers (black) in E16.5 EphA7+/− and EphA7−/− whole-mount cochleae. Scale bar: 30 μm. (C) Percentage area of space unoccupied by inner radial bundles at different stages. Data are shown as mean ±SEM. *p < 0.05; **p < 0.01; ***p < 0.001, one-way ANOVA and post hoc test. N = 10 cochleae for all genotype groups. (D–E) Images of Tuj1 stained whole-mount cochleae from EphA7+/− and EphA7−/− mice, focused on the inner spiral plexus (ISP) area for counting small fascicles entering the OC. (F–G) Tuj1 stained whole-mount cochleae from EphA7+/− and EphA7−/− mice, focused on inner radial bundles. Scale bar: 30 μm. (H) Average number of small fascicles per inner radial bundle (trunk). (I) Average number of inner radial bundles (trunks) for every 315 μm^2 image area. Data are shown as mean ±SEM. **p < 0.01; ***p < 0.001, t-test. N = 10 cochleae for all genotype groups.

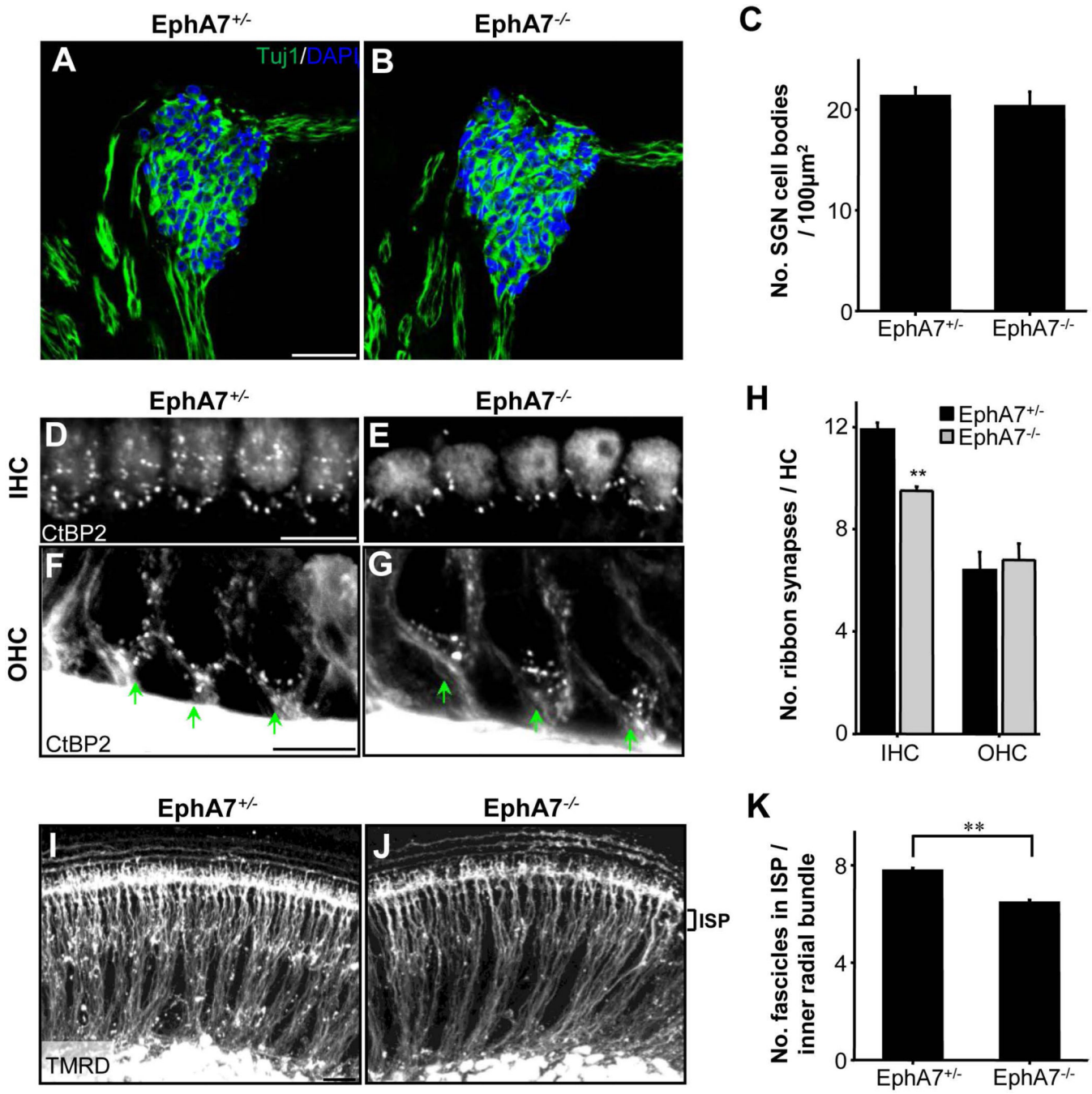

Figure 5.

Reduction in the number of synaptic contacts on inner hair cells in EphA7 deletion mice. (A–B) Representative cross-sectional images of cochleae from EphA7+/− and EphA7−/− mice at P8, immunostained with anti-Tuj (green) and DAPI (blue). Scale bar: 100 μm. (C) Average number of SGN cell bodies per 100 μm^2 area. Data are shown as mean ±SEM. N = 3 cochleae for all genotype groups. (D–E) Representative images of whole-mount cochleae from EphA7+/− and EphA7−/− mice at P8, magnified to show the IHC layer, immunostained with anti-CtBP2. Scale bar: 10 μm. (F–G) Representative images of the

cross-sectional view of cochleae from EphA7+/− and EphA7−/− mice at P8, magnified to show the OHC layer, immunostained with anti-CtBP2. Green arrow marks the base of an OHC where ribbon synapses are formed. Scale bar: 10 μm. (H) Average number of ribbon synapses per HC. Data are shown as mean ±SEM. **$p < 0.01$, t test. N = 8 cochleae for all genotype groups. (I–J) Representative images of whole-mount cochleae from EphA7+/− and EphA7−/− mice at P4, labelled with TMRD. Scale bar: 30 μm. (K) Average of number of small fascicles per inner radial bundle. Data are shown as mean ±SEM. **$p < 0.01$, t test. N = 8 cochleae for each group.

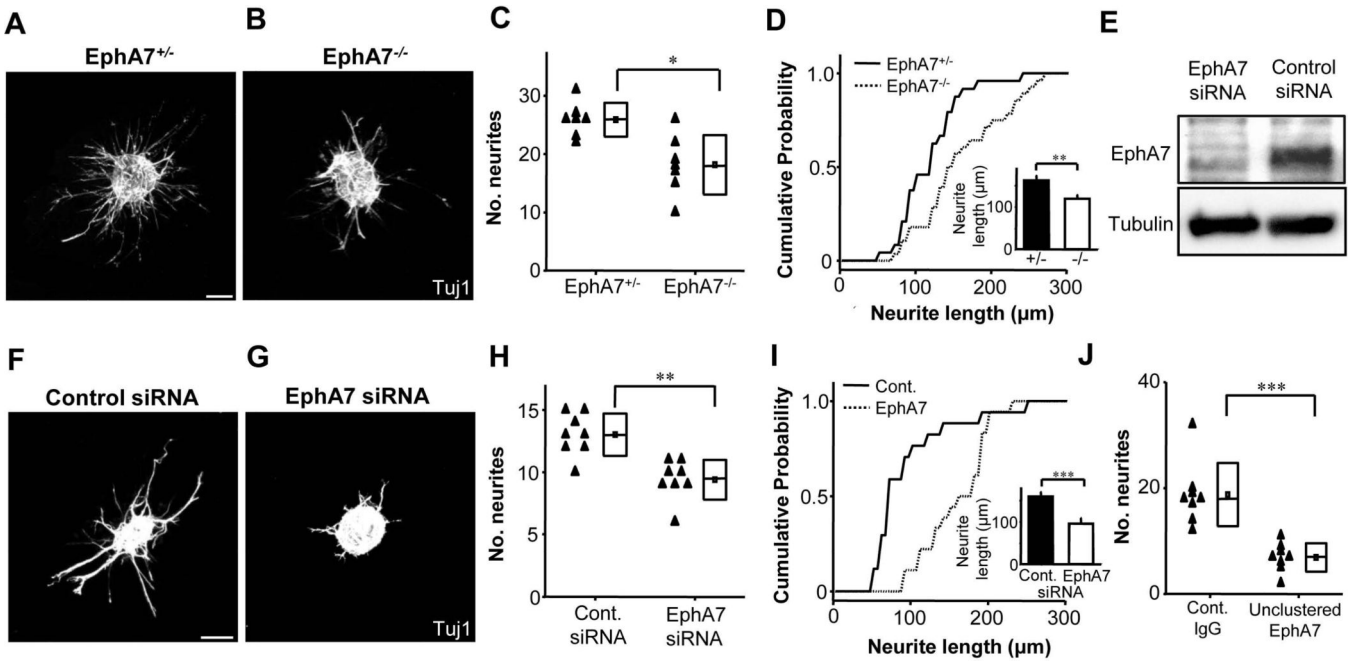

Figure 6.

EphA7 regulates outgrowth of SGN neurites. (A–B) Representative images of E16.5 SG explants from EphA7+/− and EphA7−/− mice grown *in vitro* for 4 days, immunostained with anti-Tuj1. Scale bar: 100 μm. (C) Average number of outgrown neurites per explant quantified for EphA7+/− and EphA7−/− SGs. Data are shown as mean (small box) ±SD (larger box, with the line indicating the median value). *p < 0.05, Wilcoxon rank-sum test. N = 7 explants for each genotype group. (D) Cumulative probability curve for lengths of extended neurites for explants in (C). Inset, mean neurite length quantified for EphA7+/− (n = 181) and EphA7−/− (n = 134) SG explants. Error bar = SEM. **p < 0.01, Wilcoxon rank-sum test. (E) Western blot of SG explants cultured for 4 days after electroporation of control siRNA or EphA7 siRNA. Anti-tubulin, loading control. (F–G) Images of E16.5 wild-type SG explants grown for 4 days *in vitro* after electroporation of control siRNA or EphA7 siRNA, immunostained with anti-Tuj1. Scale bar: 100 μm. (H) Average number of neurites quantified for SG explants treated with control siRNA (n = 8 explants) or EphA7 siRNA (n = 8). **p < 0.01, Wilcoxon rank-sum test. (I) Cumulative probability curve for lengths of extended neurites for explants in (H). Inset, mean neurite length quantified for control siRNA (n = 101) and EphA7 siRNA (n = 74) treated SG explants. Error bar = SEM. ***p < 0.001, Wilcoxon rank-sum test. (J) Average number of neurites quantified for SG explants treated with either control IgG (n = 8 explants) or unclustered EphA7-Fc (n = 8). ***p < 0.001, Wilcoxon rank-sum test.

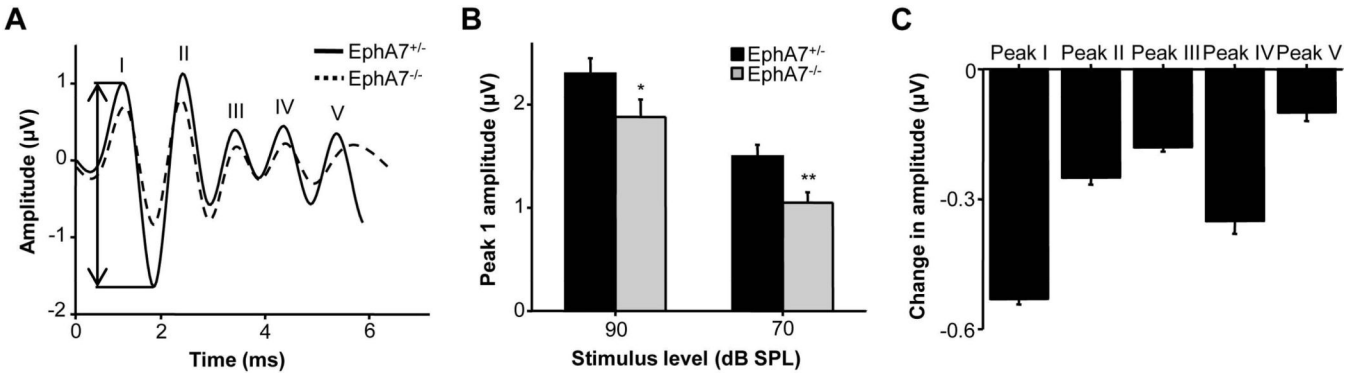

Figure 7.

Reduction of peak I amplitude of the ABR waveform in EphA7 deletion mice. (A) Traces of average ABR waveform in response to a 16 kHz tone stimulus presented at 70 dB SPL in a EphA7−/− mouse and its heterozygous littermate. Double arrow head labels the measured amplitude for peak I in the EphA7+/− mouse. Peaks I to V are marked. (B) Average peak I amplitudes at high sound intensities (70 and 90 dB SPL) for EphA7+/− and EphA7−/− mice. Data are shown as mean ±SEM. *$p < 0.05$; **$p < 0.01$, t test. N = 11 mice for each genotype. (C) Average change in amplitude for different peaks in the ABR waveform in EphA7−/− mice compared to their heterozygous littermates. 16 kHz tones at 70 dB SPL were presented. Data are shown as mean ±SEM.

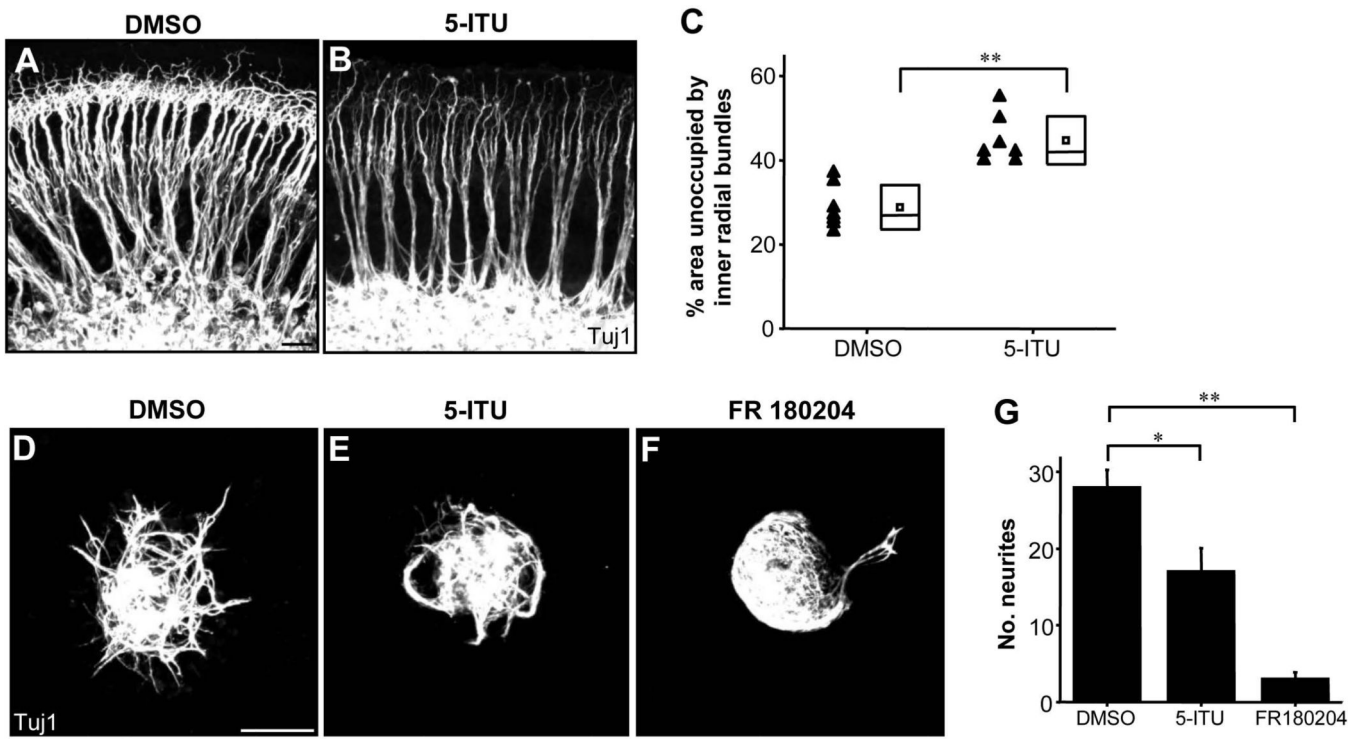

Figure 8.

Involvement of ERK1/2 activity in EphA7 signaling. (A–B) E17.5 wild-type cochleae cultured for 48 hours in the presence of either DMSO (vehicle) or 5-Iodotubercidin (5-ITU), immunostained with anti-Tuj1. Scale bar: 30 μm. (C) Quantification of percentage area of space unoccupied by inner radial bundles in cultured cochleae treated with DMSO (n = 7) or 5-ITU (n = 7). Data are shown as mean (small box) ±SD (larger box, with the line indicating the median value). **p < 0.01, t test. (D–F) E13.5 wild-type SG explants cultured in the presence of DMSO, 5-ITU or FR 180204 for 48 hours, stained with anti-Tuj1. Scale bar: 100 μm. (G) Quantification of average number of neurites per SG explant. Data are shown as mean ±SEM. *p < 0.05; **p < 0.01, t test. N = 4 explants for each group.

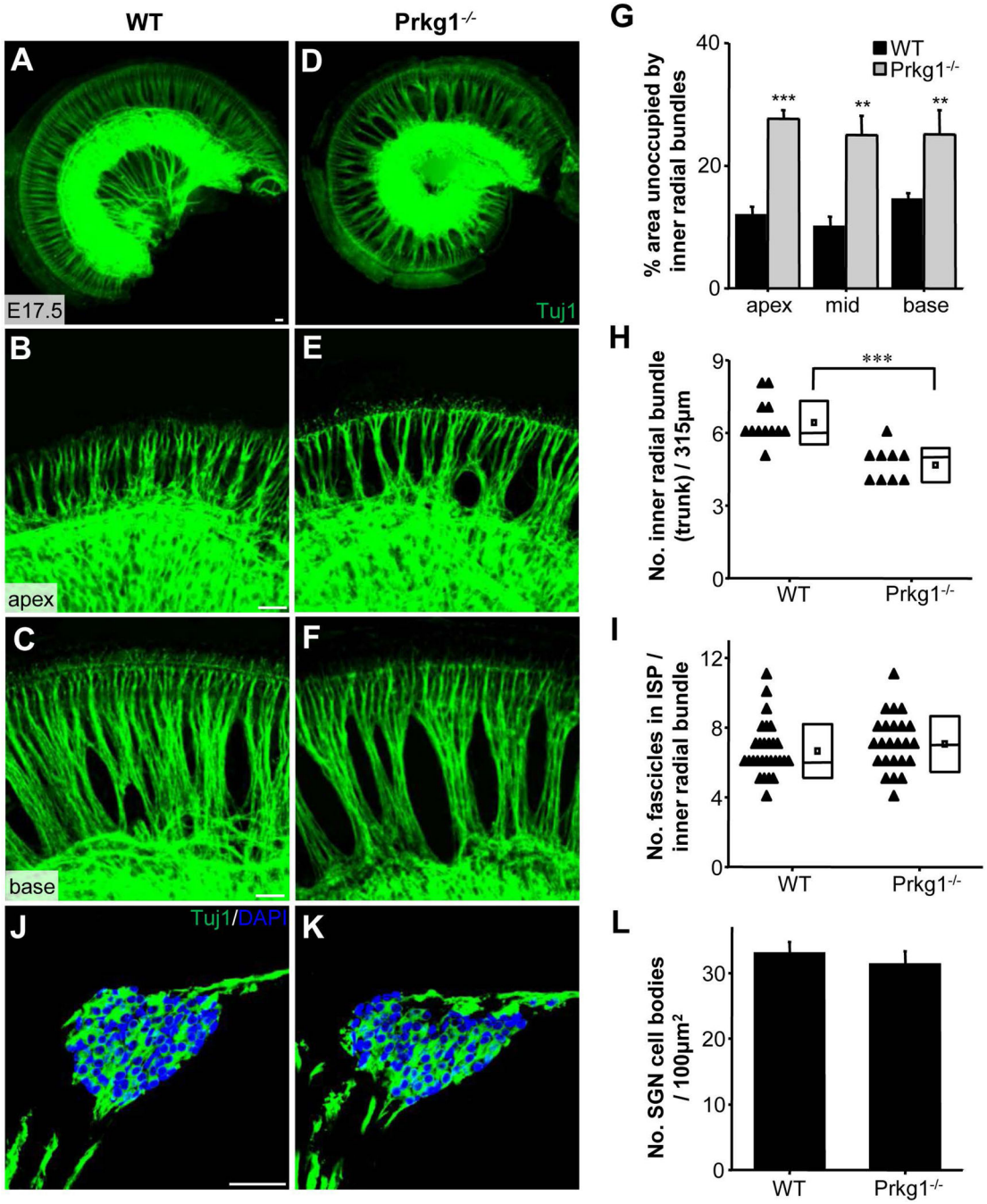

Figure 9.

Possible involvement of Prkg1. (A–F) Representative images of E17.5 whole-mount cochleae, immunostained with anti-Tuj1, from wild-type and Prkg1−/− mice, as well as higher magnification images focused on the apex and base part. All scale bars: 30 µm. (G) Percentage area of space unoccupied by inner radial bundles in the apex, mid, and base part of the cochlea. Data are shown as mean ±SEM. **$p < 0.01$; ***$p < 0.001$, t test. N = 10 cochleae for each group. (H) Quantification of average number of inner radial bundles per 315 μm^2 image area. ***$p < 0.001$, t test. (I) Average number of small fascicles per inner

radial bundle. (J–K) Representative cross-sectional images of cochleae from wild-type and Prkg1−/− mice at E17.5, immunostained with anti-Tuj (green) and DAPI (blue). Scale bar: 100 μm. (L) Quantification of average number of SGN somata per 100 μm^2 area. Data are shown as mean ±SEM. N = 3 cochleae for all genotype groups.